Mechanism and Machine Theory 179 (2023) 105115

Contents lists available at ScienceDirect

Mechanism and Machine Theory

journal homepage: www.elsevier.com/locate/mechmt

Research paper

An exact system of generation for face-hobbed hypoid gears: Application to high reduction hypoid gear drives

Ignacio Gonzalez-Perez [a,*], Alfonso Fuentes-Aznar [b]

[a] Department of Mechanical Engineering, Materials and Manufacturing, Universidad Politécnica de Cartagena, Spain
[b] Department of Mechanical Engineering, Rochester Institute of Technology, USA

ARTICLE INFO

Keywords:
High reduction hypoid gears
Face-hobbing
Tooth contact analysis
Stress analysis

ABSTRACT

The determination of the pitch cones for hypoid gears is already well defined either through numerical methods as those shown in the Standard ANSI/AGMA ISO 23509-B17 or through algorithms available in the specialized literature. However, a procedure to determine the gear tooth surfaces for hypoid gears directly from their pitch cones is still missing. An analytical approach to determine the basic machine-tool settings for the pinion and the wheel of hypoid gear drives is proposed here. It is based on the condition of exact generation, which means that the gears will operate under conjugate condition. It can be applied for generation of face-hobbed hypoid gears, produced either by the CycloCut or the CycloPalloid generation methods. A numerical example proves the goodness of the proposed methodology in a high reduction hypoid gear drive. The results of tooth contact and stress analyses prove that the bearing contact is localized and stable against misalignments, requiring just a small adjustment through the application of an optimum tip relief to the gear tooth surfaces to minimize the maximum contact pressure.

1. Introduction

High reduction hypoid gears are used in those applications where a high gear ratio and a compact design are required. An example of application of high reduction hypoid gears can be found in [1] where high reduction face-milled hypoid gears are used in the transmission of an electric vehicle. The need for application of high gear ratios in a single stage transmission for electric vehicles arises due to the high shaft velocities provided by electric motors that can reach 10,000 rpm. High reduction hypoid gears can provide gear ratios that vary typically from 1:10 to 1:50 [2] and therefore they represent an appropriate solution for the transmission of an electric vehicle as long as reverse loading would be feasible.

The first step in the design of a hypoid gear drive is the definition of the pitch cones. This definition has been actually a subject of intensive research. Basically, the available algorithms in the literature try to obtain the pitch angles, the spiral angles, and the mean pitch radii of pinion and wheel for a hypoid gear drive given the desired gear ratio and offset. There is no a unique solution since an infinite number of locations of the pitch point are possible. One of the first publications [3] dealt with the determination of basic geometric relationships in hypoid gear sets such as the condition of tangency of the tooth surfaces at the pitch point. The concepts of limit pressure angle and limit curvature for the design of the pitch cones were developed in [4,5] and the pitch cones were obtained through a trial-and-error procedure. Nowadays, a similar approach is applied in the Standard ANSI/AGMA ISO

* Corresponding author.
E-mail address: ignacio.gonzalez@upct.es (I. Gonzalez-Perez).

https://doi.org/10.1016/j.mechmachtheory.2022.105115
Received 22 July 2022; Received in revised form 16 September 2022; Accepted 27 September 2022
Available online 11 October 2022

Nomenclature

a	Hypoid offset
a_{tri}, a_{tro}	Parabola coef. for tip relief
b_1, b_2	Face width
c_{ham}	Mean addendum factor of wheel
d_{e1}, d_{e2}	Outer pitch diameter
d_{m1}, d_{m2}	Mean pitch diameter
h_{ae1}, h_{ae2}	Outer addendum
h_{fe1}, h_{fe2}	Outer dedendum
h_r	Blade reference height
h_{tri}, h_{tro}	Height for tip relief
k_c	Clearance factor
k_d	Depth factor
m_b	Blade module
m_{mn}	Mean normal module
m_{ot}	Outer transverse module
m_{1b}, m_{2b}	Roll-to-blade ratio
m_{1c}, m_{2c}	Roll-to-cradle ratio
q_{10}, q_{20}	Cradle angle
r_b	Blade base radius
r_{c0}	Cutter radius
R_{e1}, R_{e2}	Outer cone distance
R_{m1}, R_{m2}	Mean cone distance
r_{m1}, r_{m2}	Mean pitch radius
r_t	Tip edge radius
S_{r1}, S_{r2}	Radial distance
t_{z1}, t_{z2}	Pitch apex beyond crossing point
z_1, z_2	Tooth number
z_0	Number of blade groups
α_{ib}, α_{ob}	Blade pressure angle
β_{m1}, β_{m2}	Mean spiral angle
β_{m12}	Offset angle in pitch plane
ΔE_{m1}, ΔE_{m2}	Blank offset
ΔX_{B1}, ΔX_{B2}	Sliding base
ΔX_{D1}, ΔX_{D2}	Machine center to back
δ_1, δ_2	Pitch angle
γ_{m1}, γ_{m2}	Machine root angle
η	Wheel offset angle in axial plane
ν	Slope angle
ξ	Pinion offset angle in axial plane
Σ	Shaft angle

23509-B17 [6]. In [7], the relations between the pitch cone angles, the spiral angles, and the pitch radii were obtained through the solution of a system of three non-linear equations established from the conditions of meshing of the tooth surfaces at the pitch point and the location of the cutters on the pitch plane. This algorithm was valid for hypoid gears with orthogonal axes and was an improvement respect to the previous trial-and-error algorithm described in [4,5]. Later, in [8], the algorithm was simplified through the consideration of a system with just two non-linear equations for any shaft angle of the hypoid gear set. This algorithm considers as variables the pinion and wheel offset angles, whereas the pinion spiral angle and the wheel pitch radius are considered as given. A modification of the pitch cones was proposed in [9] to balance the contact ratio between the driving and coast sides using the pitch angles as variables. An optimization of the axial and radial forces in hypoid gears was presented in [10]. In hypoid gear sets with low shaft angle and face-milling as cutting method, a procedure to design the pitch cones and derive the machine-tool settings was presented in [11] whereas a procedure to define the limits of the main design parameters such as the gear ratio, the gear pitch diameter, the cutter radius, the offset, and the shaft angle was presented in [12]. Recently, a design method to minimize the contact stress in hypoid gears through the determination of some basic gear parameters was presented in [13].

The derivation of the basic machine-tool settings that allows the gear tooth surfaces to be determined for a given design of the pitch cones is another line of research. Most of the available literature refers to classical generators to define the so-called basic machine-tool settings. These basic settings can be easily transformed to be used in modern numerical control machines.

It is necessary to distinguish between the face-milling and the face-hobbing methods. In face-milling, the first publications tried to define a computational method to derive the tooth surfaces using a tilt angle and a swivel angle [14] or through the use of modified roll [15], besides some other basic machine-tool settings. A complete review of the involved basic machine-tool settings in face-milling is presented in [16].

Regarding the face-hobbing method, a first computational method to derive the tooth surfaces from the basic machine-tool settings was presented in [17]. Here, the Gleason's process was considered and it consists on the application of a single head-cutter with inner and outer blades assembled on it. Later, in [18], the model was improved to correct manufacturing errors through the modification of the basic machine-tool settings.

In all publications mentioned above related to face-milling and face-hobbing, the goal was to obtain a reliable computerized model to derive the tooth surfaces and to compute the contact pattern, the transmission errors, and the sensitivity of the contact pattern to the appearance of errors of alignment. In other words, the computerized models require the basic machine-tool settings to be known. Subsequent publications were directed to optimize the gear drive performance through the modifications of the basic machine-tool settings, such as in [19] to optimize the loaded contact pattern in face-milled hypoid gear sets, or in [20] to compensate manufacturing errors through the modification of the basic machine-tool settings of the face-milled pinion.

An interesting line of research emerged to obtain the basic machine-tool settings directly from the basic gear parameters such as the pitch cone and tooth macro-geometry data. In [21], an approach was proposed to derive the basic machine-tool settings of a spiral bevel or a hypoid wheel, either in face-milling or face-hobbing, generated or non-generated, from the basic gear drive data. Once the wheel is obtained, it is possible to synthesize the pinion in some cases. In [22], local synthesis is applied to get the basic machine-tool settings of a face-milled spiral bevel pinion. In [23], an alternative approach based on the consideration of a face-milled spiral bevel pinion as a conjugate of the wheel is developed. Most techniques such as those based on local synthesis or ease-off have been focused mainly on face-milling to synthesize the pinion tooth surfaces from the wheel tooth surfaces.

In [24] the basic machine-tool settings were derived directly for both members of a spiral bevel and a hypoid gear drive considering a face-hobbed non-generated wheel and a face-hobbed generated pinion. Such work showed that line contact and zero unloaded transmission errors were possible either in a spiral bevel or a hypoid gear drive when face-hobbing with a non-generated wheel is considered. In [25], two face-hobbing methods, the Cyclo-Cut™ and the Cyclo-Palloid™, were illustrated and compared as methods of generation of spiral bevel gears.

The presented research fills a gap between the pitch cones, obtained through known algorithms, and the determination of the basic machine-tool settings for both members of a hypoid gear drive. This determination is analytical, direct, and based on an exact system of generation that does not yield unloaded transmission errors. The exact system of generation is somehow linked to face-hobbing where both members of the hypoid gear drive are generated (see [26]). The methodology can be applied either in Cyclo-Cut™ gears or in Cyclo-Palloid™ gears. The developed theory is applied to a high reduction hypoid gear drive with orthogonal axes, although it can be extended to non-orthogonal axes. The results of tooth contact analysis and stress analysis will show that a localized bearing contact with no unloaded transmission errors and stable contact pattern against misalignments is feasible. Such contact pattern requires just a small adjustment through the application of a tip relief to the gear tooth surfaces to avoid areas of severe contact.

The definition of the pitch cones implies the computation of the pinion and wheel mean cone distances, R_{m1} and R_{m2}, both pitch angles δ_1 and δ_2, and the mean spiral angles β_{m1} and β_{m2}. The nomenclature corresponds to that used in the Standard ANSI/AGMA ISO 23509-B17 [6]. Fig. 1(a) shows such data for an example of a hypoid gear drive. Here, a is the hypoid offset, d_{m1} and d_{m2} are the mean pitch diameters, and $\beta_{m12} = \beta_{m1} - \beta_{m2}$. The configuration represented in Fig. 1(a) is the starting step of the presented research that pursues the materialization of the tooth surfaces on the pitch cones illustrated in Fig. 1(b) with the above mentioned favorable conditions of contact.

2. Determination of the pitch cones and the pitch plane

The required data for the determination of the pitch cones can be slightly different among the different approaches described in the previous section, but basically it consists of the hypoid offset a, the shaft angle Σ, the number of teeth z_1 and z_2, the wheel mean pitch diameter d_{m2}, the wheel face width b_2, the pinion spiral angle β_{m1}, the cutter radius r_{c0} and, for the face-hobbing processes, the number of blade groups z_0. The selection of d_{m2} and b_2 allows the size of the transmission to be set. However, in some cases the wheel outer pitch diameter d_{e2} is considered instead of d_{m2}. On the other hand, some methods in the Standard ANSI/AGMA ISO 23509-B17 [6] considers the wheel mean spiral angle β_{m2} as an input instead of β_{m1}. However, β_{m1} would be preferable as an input data in high reduction hypoid gear drives to have a major control on the pinion helix angle and avoid the self-locking effect of the transmission. Angle β_{m1} is considered as input data in the approaches represented in [7,8].

The determination of the pitch cones implies the positioning of the pitch point P (see Fig. 1(a)). Point P and the two generatrices of the pitch cones (with lengths R_{m1} and R_{m2}) form the pitch plane. The determination of the pitch plane is important for the methodology proposed in this paper since it constitutes the plane of motion of the cradle and the cutter in the generating face-hobbing process.

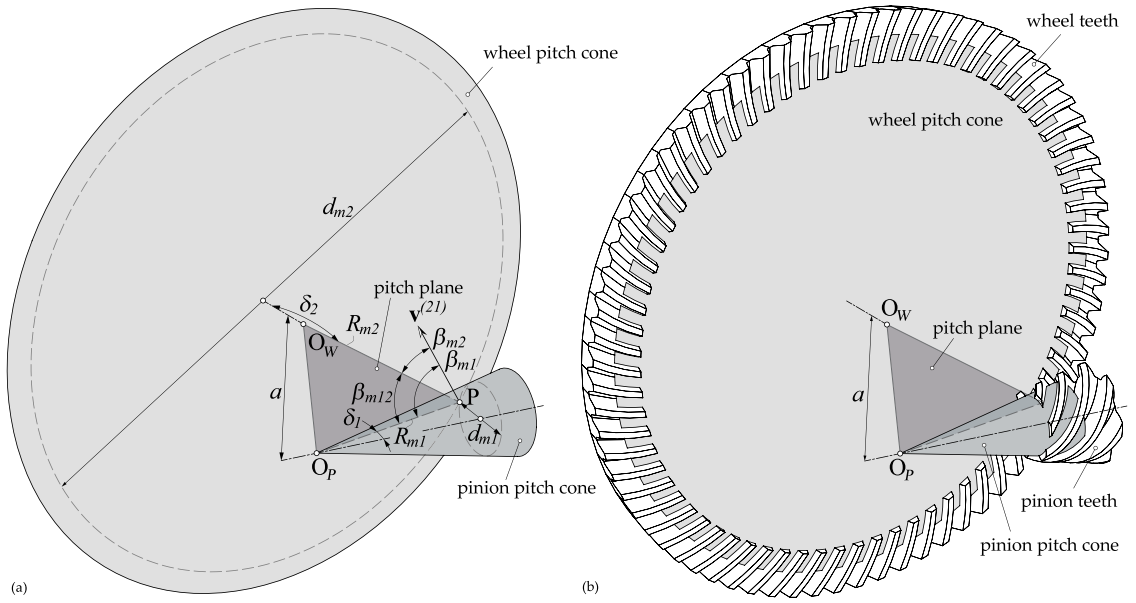

Fig. 1. Hypoid pitch cones: (a) representation of the pitch plane and (b) representation of the pitch cones and the to-be-determined gear tooth surfaces.

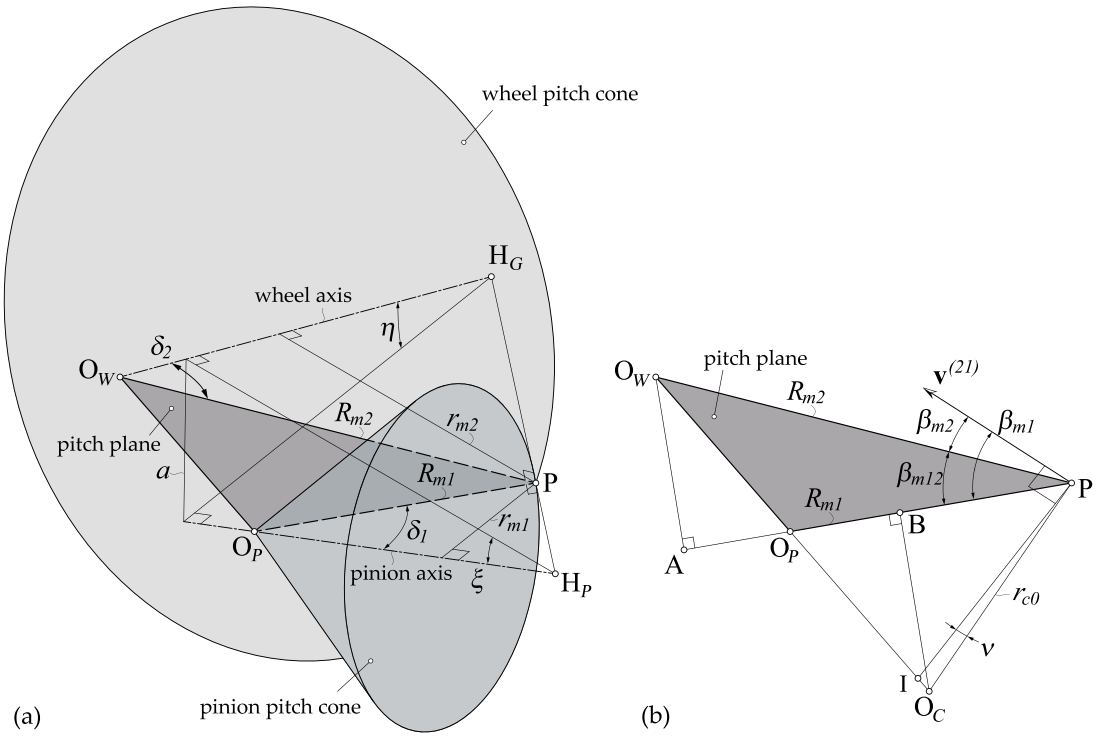

Fig. 2. The pitch plane with illustration of: (a) offset angles ξ and η and (b) alignment of O_C with O_W and O_P.

The applied approach for the determination of the pitch cones is similar to that represented in [8] where just the solution of two non-linear equations with two unknowns, namely, the offset angles at the axial planes ξ and η (see Fig. 2(a)) is required. The first equation represents the condition of meshing of the hypoid gears at the pitch point:

$$f_1(\xi,\eta) = r_{m1}(\xi,\eta) z_2 \cos\beta_{m1} - r_{m2} z_1 \cos\beta_{m2}(\xi,\eta) = 0 \tag{1}$$

where r_{m1} and r_{m2} are the mean pitch radii, and the second equation is particular for face-hobbing processes and implies that the cutter, which has a given cutter radius r_{c0}, has its center O_C aligned with the pitch apexes O_P and O_W (see Fig. 2(b)):

$$f_2(\xi,\eta) = \overline{O_W A} \cdot \overline{O_P B} - \overline{O_P A} \cdot \overline{O_C B} = 0 \tag{2}$$

with

$$\overline{O_W A} = R_{m2}(\xi,\eta)\sin\beta_{m12}(\xi,\eta) \tag{3}$$

$$\overline{O_P B} = R_{m1}(\xi,\eta) - r_{c0}\sin(\beta_{m1} - \nu(\xi,\eta)) \tag{4}$$

$$\overline{O_P A} = R_{m2}(\xi,\eta)\cos\beta_{m12}(\xi,\eta) - R_{m1}(\xi,\eta) \tag{5}$$

$$\overline{O_C B} = r_{c0}\cos(\beta_{m1} - \nu(\xi,\eta)) \tag{6}$$

Here, ν is the slope angle of the cutter,

$$\nu(\xi,\eta) = \arcsin\left(\frac{m_b(\xi,\eta)z_0}{2r_{c0}}\right) \tag{7}$$

where z_0 is the number of blade groups of the cutter and m_b is the blade module, which is equal to the mean normal module $m_{mn} = d_{m2}\cos\beta_{m2}(\xi,\eta)/z_2$.

In this approach, the Wildhaber's limiting condition [4] is not applied, although designers have to take precautions to keep the pressure angles far from the limiting pressure angle (basically computing the limiting pressure angle, for example according to [7,8], and avoiding some cutter radii).

The relations of the design variables as a function of angles ξ and η can be found in specialized literature [8] and are particularized here for a shaft angle of 90 degrees:

$$r_{m1}(\xi,\eta) = \frac{a - r_{m2}\sin\xi}{\sin\eta} \tag{8}$$

$$\delta_1(\xi,\eta) = \arctan\left(\frac{\sin\eta}{\tan\xi}\right) \tag{9}$$

$$\delta_2(\xi,\eta) = \arctan\left(\frac{\sin\xi}{\tan\eta}\right) \tag{10}$$

$$\beta_{m12}(\xi,\eta) = \arccos(\tan\delta_1(\xi,\eta)\tan\delta_2(\xi,\eta)) \tag{11}$$

$$\beta_{m2}(\xi,\eta) = \beta_{m1} - \beta_{m12}(\xi,\eta) \tag{12}$$

$$R_{m1}(\xi,\eta) = \frac{r_{m1}(\xi,\eta)}{\sin\delta_1(\xi,\eta)} \tag{13}$$

$$R_{m2}(\xi,\eta) = \frac{r_{m2}}{\sin\delta_2(\xi,\eta)} \tag{14}$$

3. An exact system of generation of pinion and wheel

The basic machine-tool settings for pinion and wheel have to be determined to guarantee an exact system of generation, which means that pinion and wheel will rotate without unloaded transmission errors (conjugate action). In order to get this exact system of generation, it is required that (see [26]):

(1) The cradles for generation of pinion and wheel have collinear axes.
(2) The head-cutters for generation of pinion and wheel have collinear axes.
(3) The pinion outer blades and wheel inner blades (respectively, pinion inner blades and wheel outer blades) have congruent blade profiles.

The configuration of this system of generation can be visualized in Fig. 3 where both head-cutters, both cradles, and the pitch plane have been represented. The rotations of the cradles and the head-cutters occur parallel to the pitch plane. Congruent profiles can also be observed on a detailed view of the plane that contains the front faces of the blades. Such a system will provide a gear drive with no backlash. In face-hobbing, the backlash and tooth thickness can be controlled throughout the application of an offset angle between the inner and the outer blades without affecting the contact conditions.

The velocity of the pitch point P as a point of any of the cradles has to coincide with the velocity of the same point as belonging to the wheel, $\mathbf{v}_P^{(cr1)} = \mathbf{v}_P^{(cr2)} = \mathbf{v}_P^{(2)}$. This condition yields

$$\omega_{cr2} = \omega_2\frac{r_{m2}}{R_{m2}} = \omega_2\sin\delta_2 \tag{15}$$

$$\omega_{cr1} = \omega_{cr2} = \omega_2\sin\delta_2 = \omega_1\frac{z_1}{z_2}\sin\delta_2 \tag{16}$$

At the pitch point P, the wheel and its corresponding cradle have pure rolling. However, at the same point P, the pinion and its cradle have rolling and sliding. The sliding velocity $\mathbf{v}_P^{(12)}$ results tangent to the pinion tooth surface and therefore to the gear tooth surface too.

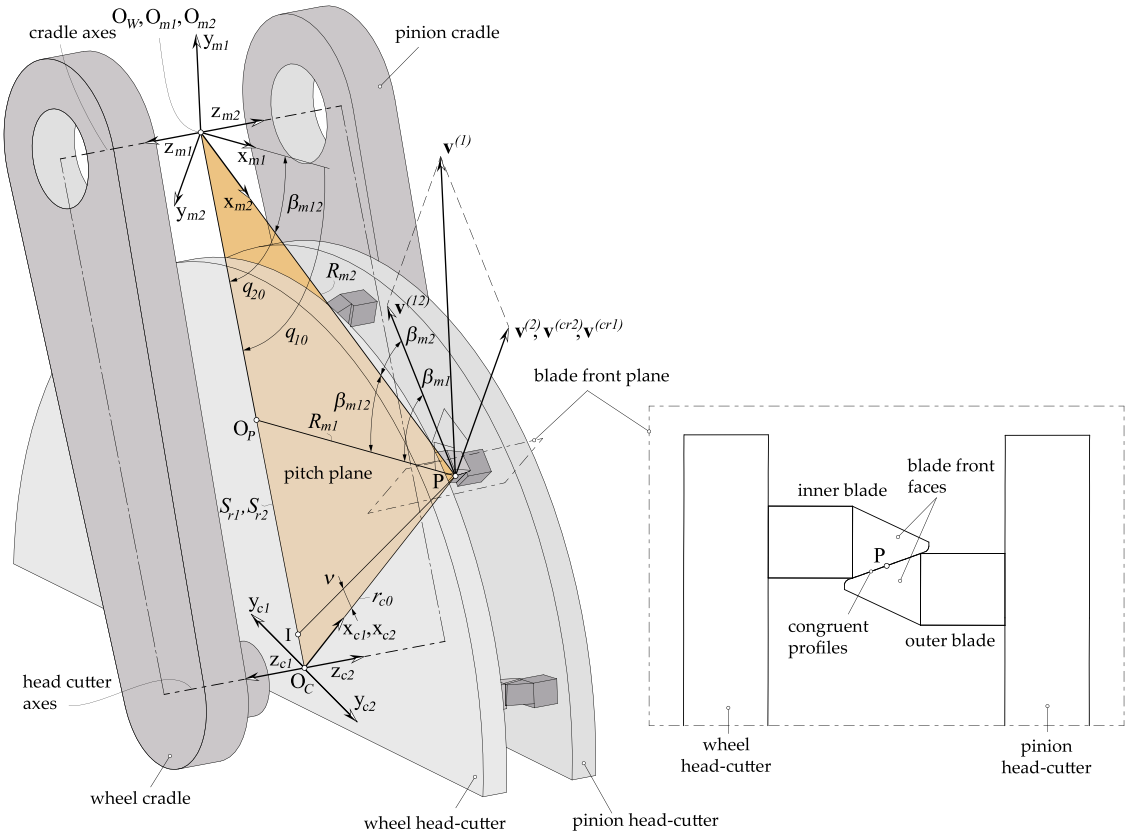

Fig. 3. Configuration of the position of cradles and head-cutters for an exact system of generation of hypoid gears.

On the other hand, the velocity of the head-cutter ω_{c1} (respectively, ω_{c2}) is related to ω_{cr1} (respectively, ω_{cr2}) and therefore to the rotation of the pinion ω_1 (respectively, of the wheel ω_2). The instantaneous center of relative rotation of any of the head-cutters respect to its corresponding cradle is represented by point I. The segment $\overline{\text{IP}}$ has to be perpendicular to the sliding velocity $\mathbf{v}_P^{(12)}$ (that is also the cutting velocity). The segment $\overline{\text{IP}}$ is contained in the plane of the front faces of the blades. The following relations have to be satisfied:

$$\omega_{c1} = \omega_1 \frac{z_1}{z_0} \tag{17}$$

$$\omega_{c2} = \omega_2 \frac{z_2}{z_0} \tag{18}$$

Fig. 3 shows the configuration of the machine coordinate systems S_{m1} and S_{m2} that allows, through the sough-for machine tool settings, the positioning of the head-cutters, the pinion, and the wheel to be determined. The Appendix illustrates some basic concepts related to the blades, the cutter, the cradle, and their assembly in a cutting machine for a generated face-hobbing process.

4. Determination of the basic machine-tool settings of the wheel

The basic machine-tool settings of the wheel are established through the location of the wheel and the cutter in the machine coordinate system S_{m2}. Fig. 4 shows the configuration of system S_{m2}, where its origin O_{m2} coincides with the wheel pitch cone apex O_W and its axis x_{m2} is aligned with the pitch cone generatrix that passes through the pitch point P. The axis z_{m2}, not represented in Fig. 4, is directed normal to the pitch plane.

Since O_{m2} coincides with O_W, the machine center to back ΔX_{D2}, the sliding base ΔX_{B2} and the blank offset ΔE_{m2} (see Appendix) are all equal to zero. Additionally, the machine root angle γ_{m2} coincides with the wheel pitch cone angle δ_2.

On the other hand, the head-cutter is set on the cradle with its center of rotation O_C located at a radial distance S_{r2} from the center of rotation of the cradle O_{cr2} and at an initial cradle angle q_{20}

$$S_{r2} = \sqrt{R_{m2}^2 + r_{c0}^2 + 2R_{m2}r_{c0}\sin(\beta_{m2} - \nu)} \tag{19}$$

$$q_{20} = \arcsin\left(\frac{r_{c0}\cos(\beta_{m2} - \nu)}{S_{r2}}\right) \tag{20}$$

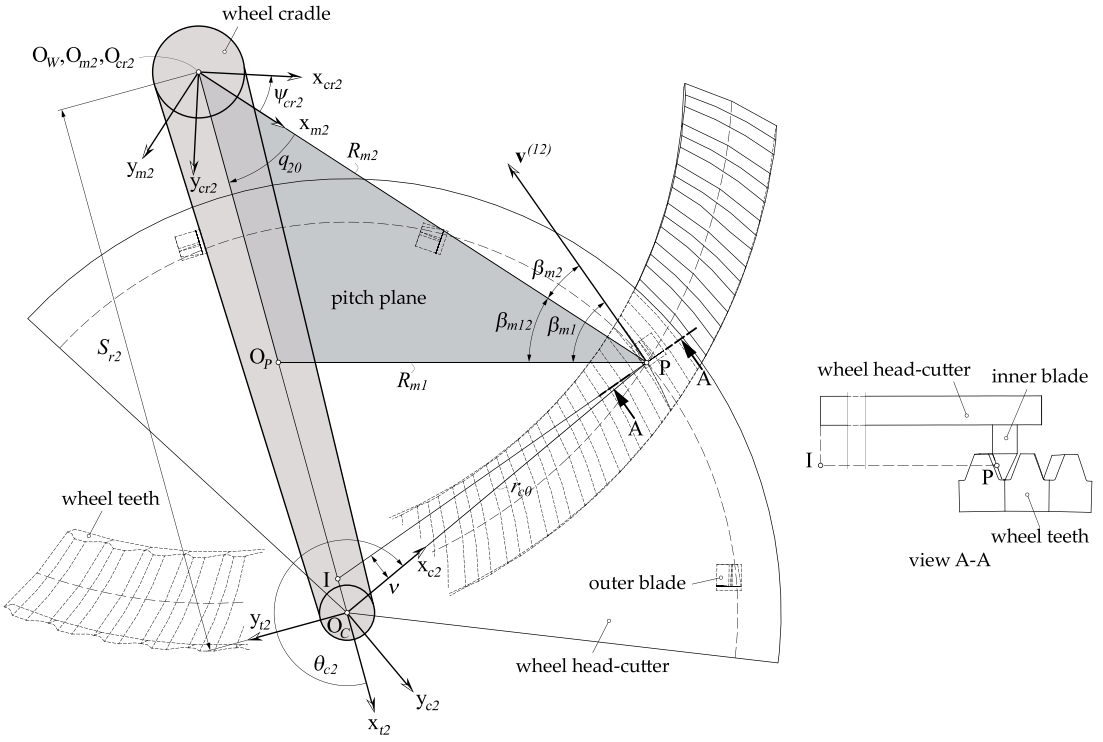

Fig. 4. For illustration of the basic machine-tool settings of the wheel.

The rotation of the cradle ψ_{cr2} and the rotation of the cutter θ_{c2} are plane motions parallel to the pitch plane. Both rotations are opposite since the instantaneous center of relative rotation, point I, is located between centers O_{cr2} and O_C. Both rotations are related to the rotation of the wheel ψ_2 through

$$\psi_2 = \psi_{cr2} m_{2c} + \theta_{c2} m_{2b} \tag{21}$$

where m_{2c} is the velocity ratio or roll-to-cradle ratio

$$m_{2c} = \frac{R_{m2}}{r_{m2}} = \frac{1}{\sin \delta_2} \tag{22}$$

and m_{2b} is the roll-to-blade ratio

$$m_{2b} = \frac{z_0}{z_2} \tag{23}$$

5. Determination of the basic machine-tool settings of the pinion

Fig. 5 shows the setting of system S_{m1} for the determination of the pinion basic machine-tool settings. Origin O_{m1} coincides with the wheel pitch cone apex O_W. Axis x_{m1} is contained in the pitch plane and is kept parallel to the generatrix of the pinion pitch cone that passes through the pitch point P. Axis z_{m1}, not represented in Fig. 5, is normal to the pitch plane.

Since O_{m1} does not coincide with the pinion pitch cone apex O_P, the settings ΔX_{D1}, ΔX_{B1} and ΔE_{m1} are not zero but given by the following relations:

$$\Delta E_{m1} = -\overline{O_{m1}Q} = -R_{m2} \sin \beta_{m12} \tag{24}$$

$$\Delta X_{B1} = \overline{QR} = (R_{m2} \cos \beta_{m12} - R_{m1}) \tan \delta_1 \tag{25}$$

$$\Delta X_{D1} = \overline{RO_P} = (R_{m2} \cos \beta_{m12} - R_{m1}) / \cos \delta_1 \tag{26}$$

Furthermore, the machine root angle γ_{m1} coincides with the pinion pitch cone angle δ_1. The cradle, no represented in Fig. 5, is located as in Fig. 4 with its center of rotation O_{cr1} located at the pitch cone apex O_W of the wheel. The head-cutter also takes the same position as in Fig. 4, but with the blades pointing in opposite direction (see Fig. 3). Then, the radial distance S_{r1} and the initial cradle angle q_{10} are given as

$$S_{r1} = S_{r2} \tag{27}$$

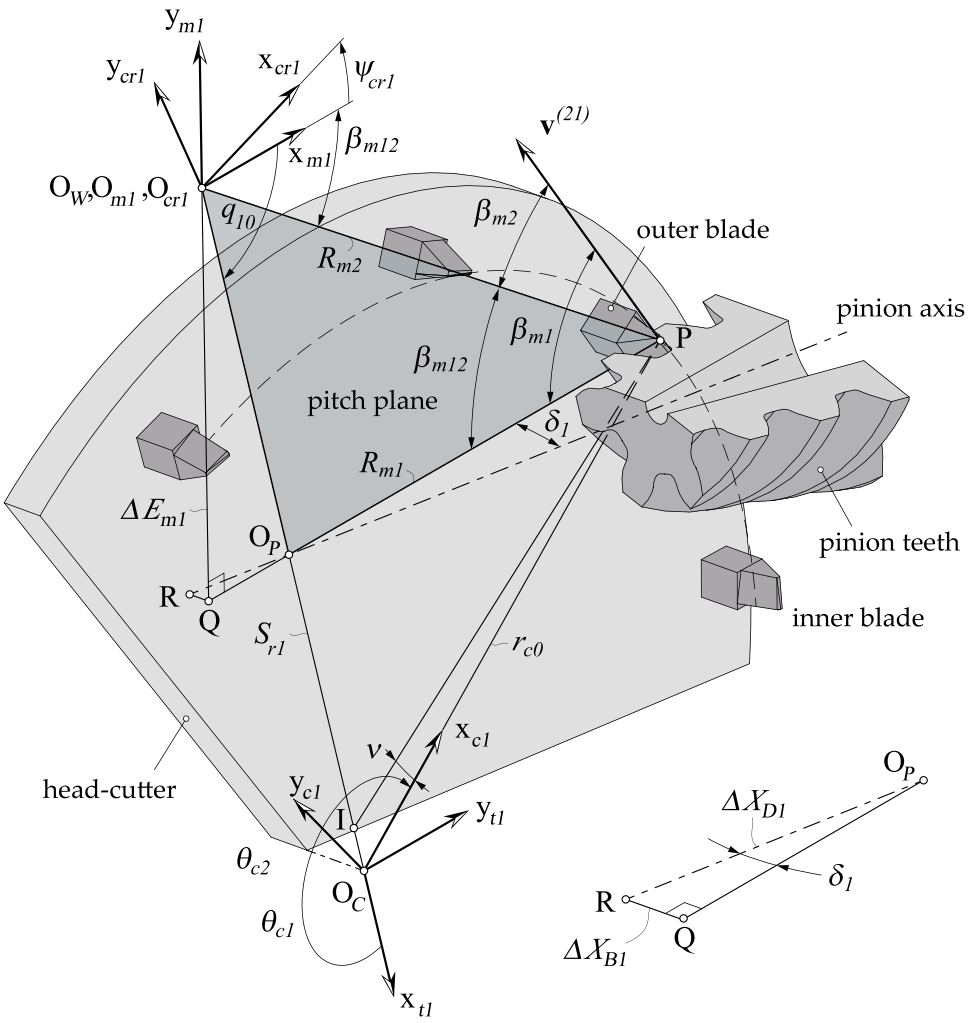

Fig. 5. For illustration of the basic machine-tool settings of the pinion.

$$q_{10} = q_{20} + \beta_{m12} \tag{28}$$

As for the wheel, the rotation of the cradle ψ_{cr1} is opposite to the rotation of the cutter θ_{c1}. Both rotations are related to the rotation ψ_1 of the pinion through

$$\psi_1 = \psi_{cr1} m_{1c} + \theta_{c1} m_{1b} \tag{29}$$

where m_{1c} is the velocity ratio or roll-to-cradle ratio

$$m_{1c} = \frac{1}{\sin\delta_2}\frac{z_2}{z_1} \tag{30}$$

and m_{1b} is the roll-to-blade ratio

$$m_{1b} = \frac{z_0}{z_1} \tag{31}$$

6. Numerical example

The following numerical example proves that feasible tooth surfaces with favorable conditions of meshing and contact can be obtained after application of the proposed methodology. The starting point for application of the proposed methodology is the positioning and dimensioning of the pitch cones of the hypoid gear drive, that can be given or can be determined from basic gear drive data as shown in Section 2. Table 1 shows the initial data for the determination of the pitch cones. In this case, a high reduction hypoid gear drive with a gear ratio 1:12.167 has been considered.

Table 1
Basic input data for the hypoid pitch cone determination.

Data	Pinion	Wheel
Tooth numbers, z_1 and z_2	6	73
Shaft angle, Σ [°]	90.0	
Pinion offset, a [mm]	55.0	
Wheel mean pitch radius, r_{m2} [mm]		130.0
Wheel face width, b_2 [mm]		35.0
Pinion spiral angle, β_{m1} [°]	65.0	
Cutter radius, r_{c0} [mm]	100.0	
Number of blade groups, z_0	5	
Mean addendum factor of wheel[a], c_{ham}		0.5
Depth factor[a], k_d		1.75
Clearance factor[a], k_c		0.125

[a]See Standard ANSI/AGMA ISO 23509-B17 [6].

Table 2
Derived basic data of the hypoid gear drive.

Data	Pinion	Wheel
Pitch angles, δ_1 and δ_2 [°]	10.791	78.152
Wheel spiral angle, β_{m2} [°]		40.308
Pinion mean pitch radius, r_{m1} [mm]	19.280	
Mean normal module, m_{mn} [mm]	2.716	
Mean pitch diameter, d_{m1} and d_{m2} [mm]	38.56	260.0
Mean cone distance, R_{m1} and R_{m2} [mm]	102.974	132.830
Pinion face width[a], b_1 [mm]	43.0	
Outer pitch diameter d_{e1} and d_{e2}	46.510	294.254
Outer transverse module, m_{ot} [mm]		4.031
Outer cone distance, R_{e1} and R_{e2} [mm]	124.205	150.330
Pitch apex beyond crossing point, t_{z1} and t_{z2} [mm]	−17.397	8.063
Outer addendum, h_{ae1} and h_{ae2} [mm]	2.377	2.377
Outer dedendum, h_{fe1} and h_{fe2} [mm]	2.971	2.971

[a]Determined according to method 3 in Standard ANSI/AGMA ISO 23509-B17 [6].

Table 3
Derived basic data of the head-cutters.

Data	Value
Blade module, m_b [mm]	2.716
Slope angle, ν [°]	3.893
Reference height, h_r [mm]	2.971
Tip edge radius[a], r_t [mm]	1.032

[a]Determined as $0.38m_{mn}$.

6.1. Determination of the pitch cones and basic gear data

Solution of the system of Eqs. (1) and (2) provides the offset angles $\xi = 24.227°$ and $\eta = 4.920°$ (see Fig. 2). Then, application of Standard ANSI/AGMA ISO 23509-B17 [6] allows the basic gear data to be derived (see Table 2). On the other hand, Table 3 shows the derived basic data for the head-cutters of pinion and wheel. A blade pressure angle $\alpha_{ib} = \alpha_{ob} = 20°$ has been considered. This angle is actually far from the calculated limiting pressure angle of the gear drive, which has a value of 0.649° [7,8] in this numerical example.

6.2. Determination of the tooth surfaces of pinion and wheel

Application of Section 4 allows the basic machine-tool settings of the wheel to be derived (see Table 4 and Fig. A.16). In the same way, application of Section 5 allows the basic machine-tool settings of the pinion to be derived (see Table 5 and Fig. A.16).

It can be observed either in Table 4 or in Table 5 that the same set of machine-tool settings are applied to both tooth sides (convex and concave). Here, CV stands for convex tooth side and CC stands for concave tooth side. This means that a Cyclo-Cut process with a head-cutter having their inner and outer blades assembled on it constitutes an appropriate method of cutting. The reason is that the methodology proposed in Sections 4 and 5 provides a localized bearing contact, as it will be illustrated next, and no crowning of the tooth surfaces is required. Therefore, the same machine-tool settings can be applied to both tooth sides and no tilting of the head-cutter is required. A Cyclo-Palloid process would be possible as well considering that both head-cutters have coincident axes and the so-called eccentricity [27] is zero.

Table 4
Basic machine-tool settings of the wheel.

Data	Wheel(CV)	Wheel(CC)
Machine center to back, ΔX_{D2} [mm]	0.0	
Sliding base, ΔX_{B2} [mm]	0.0	
Bland offset, ΔE_{m2} [mm]	0.0	
Machine root angle, γ_{m2} [°]	78.152	
Velocity ratio, m_{2c}	1.021768	
Roll-to-blade radio, m_{2b}	0.068493	
Radial distance, S_{r2} [mm]	108.966	
Cradle angle, q_{20} [°]	47.606	

Table 5
Basic machine-tool settings of the pinion.

Data	Pinion(CV)	Pinion(CC)
Machine center to back, ΔX_{D1} [mm]	18.029	
Sliding base, ΔX_{B1} [mm]	−3.376	
Bland offset, ΔE_{m1} [mm]	−55.489	
Machine root angle, γ_{m1} [°]	10.791	
Velocity ratio, m_{1c}	12.431511	
Roll-to-blade radio, m_{1b}	0.833333	
Radial distance, S_{r1} [mm]	108.966	
Cradle angle, q_{10} [°]	72.298	

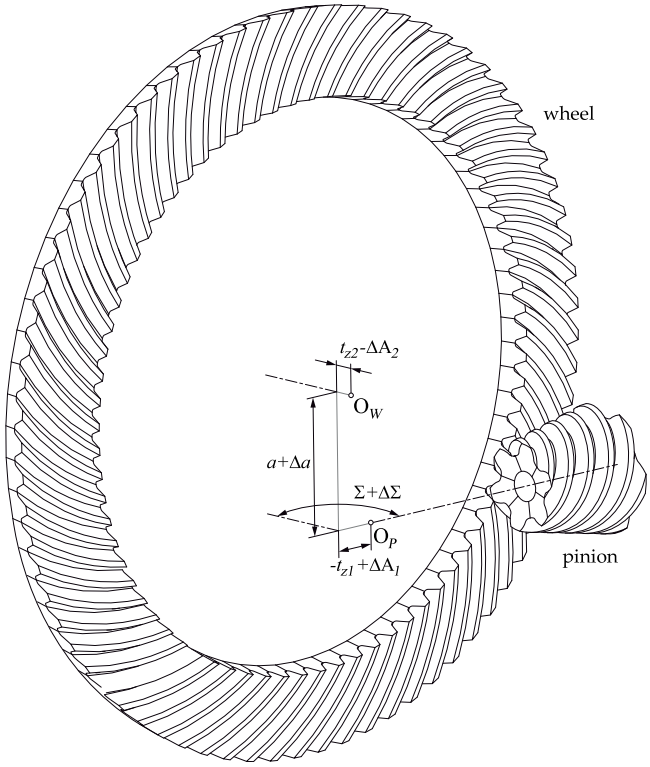

Fig. 6. Hypoid gear drive model and illustration of possible errors of alignment.

The tooth surfaces of pinion and wheel are determined by the application of the theory of gearing [16] and following the ideas exposed in Appendix. Fig. 6 shows the hypoid gear drive model where the alignment errors (that will be considered in the next section) are illustrated as well.

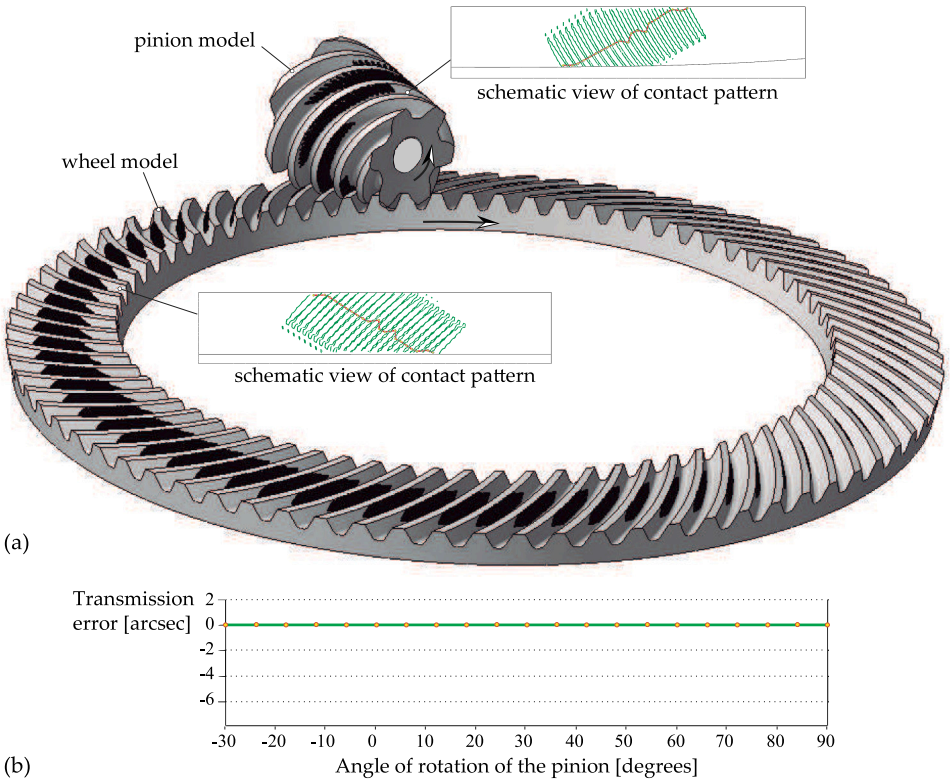

Fig. 7. Results of tooth contact analysis for a clockwise rotation of the pinion: (a) contact patterns and (b) function of unloaded transmission errors.

6.3. Tooth contact and stress analyses

Tooth contact analysis (TCA) is applied following an algorithm already published in works [24,27]. A total of 21 steps or contact positions are considered equally spaced along an angle of rotation of the pinion equal to $4\pi/z_1$ (two angular pitches) and considering a virtual marking compound thickness of 0.0065 mm for representation of the contact pattern. This algorithm considers that the tooth surfaces are rigid and a total of three pairs of tooth surfaces can contact simultaneously. Application of TCA provides the contact patterns illustrated in Fig. 7(a), represented on both the 3D model of the gear drive and schematically on a radial projection of the gear tooth surfaces, for the pinion rotating in clockwise direction causing contact on the concave tooth surfaces of the pinion and the convex tooth surfaces of the wheel. It can be observed that the bearing contact is localized and oriented in diagonal direction on the gear tooth surfaces. Fig. 7(b) confirms that the function of unloaded transmission errors is zero and conjugate action is indeed achieved.

Fig. 8 shows the results of TCA when the rotation of the pinion is in counterclockwise direction causing contact on the convex tooth surfaces of the pinion and the concave tooth surfaces of the wheel. Similar conclusions as those obtained for a clockwise rotation can be drawn.

Since no profile crowning or tip/root relief is applied to the tooth surfaces of pinion and wheel, the radial projections on Figs. 7 and 8 show that some contact ellipses are truncated and therefore high values of contact stresses are expected. In order to avoid zones of severe contact, an optimized tip relief of the teeth could be found. Fig. 9 shows some values of parabola coefficients $a_{tro}^{(P)}$ and $a_{tri}^{(W)}$ (see Fig. A.15) and their corresponding contact patterns on a radial projection of pinion concave tooth surface, considering a tip relief height $h_{tri} = h_{tro} = 1.5$ mm. Here, $a_{tro}^{(P)}$ is the parabola coefficient for the tip relief of the outer blades that generate the pinion concave tooth surfaces, and $a_{tri}^{(W)}$ is the parabola coefficient for the tip relief of the inner blades that generate the wheel convex tooth surfaces. The optimized values of parabola coefficients will depend on the applied torque that determines the real size of the bearing contact (which is not shown in Fig. 9).

The real size of the bearing contact and the values of contact pressures are determined after a finite element analysis is carried out. Fig. 10 shows the considered finite element model, that has a total of 508,118 nodes and 421,500 elements distributed in a pinion with all its teeth and in a wheel with seven teeth. The number of finite elements along the face width is 150 for the pinion and 55 for the wheel. There are 30 finite elements in profile direction for both the pinion and wheel tooth surfaces. The nodes on the lower side of the pinion rim constitute a rigid surface, that is rigidly connected to reference node O_p (the pinion pitch cone apex). All the degrees of freedom are blocked on this node, but the rotation about the pinion axis is released. A torque T is applied on that released degree of freedom, transmitting the load to the pinion through the lower side of the rim. On the other hand, the

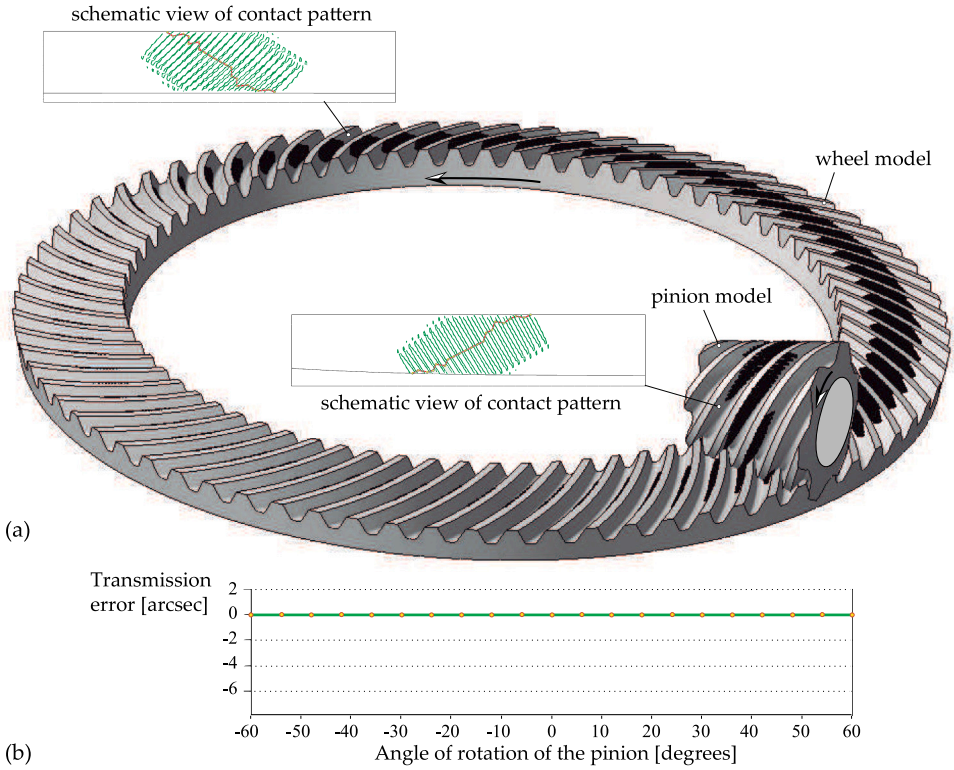

Fig. 8. Results of tooth contact analysis for a counterclockwise rotation of the pinion: (a) contact patterns and (b) function of unloaded transmission errors.

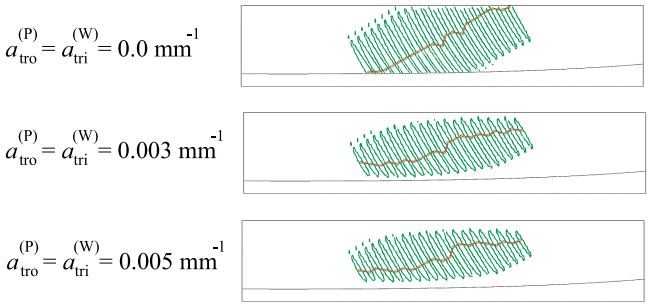

Fig. 9. Effects of tip relief on the contact pattern on pinion concave tooth surface ($h_{tri} = h_{tro} = 1.5$ mm).

nodes around the rim of the wheel form as well rigid surfaces that are rigidly connected to the reference node O_W (the wheel pitch cone apex). All the degrees of freedom are blocked on this node. However, rotation about the wheel axis is forced at each step of the analysis to investigate the evolution of the maximum contact pressure along the cycle of meshing. A total of 21 steps are considered along two angular pitches of rotation of the pinion, covering an angle equal to $4\pi/z_1$ rad. The contact interactions in the model are defined between tooth surface pairs $1^{(P)}$-$1^{(W)}$, $2^{(P)}$-$2^{(W)}$, $3^{(P)}$-$3^{(W)}$, $4^{(P)}$-$4^{(W)}$, $5^{(P)}$-$5^{(W)}$, $6^{(P)}$-$6^{(W)}$, and $1^{(P)}$-$7^{(W)}$, considering a slave–master interaction [28].

A torque $T = 110$ Nm is considered in this example. The required torque and the basic data that determines the size of the transmission, r_{m2} and b_2, are related to each other and can be found through a trial-and-error procedure with the objective to keep the maximum contact pressure below a certain value. The pinion spiral angle is also important in this procedure to guarantee a high face contact ratio that allows variable r_{m2} to be decreased. The pinion spiral angle may have also a maximum limit value if reverse loading is desired.

Fig. 11 shows the formation of the bearing contact on the pinion model at step (or contact position) 11 of a total of 21 steps when a parabola coefficient $a_{tro}^{(P)} = a_{tri}^{(W)} = 0.005$ mm^{-1} is applied. Fig. 11 shows that simultaneous contact occur in five tooth surfaces, reaching a maximum contact pressure of 1172.2 MPa.

Fig. 12 shows the evolution of the maximum contact pressure for the case $a_{tro}^{(P)} = a_{tri}^{(W)} = 0.005$ mm^{-1}, indicating its value at each tooth pair and for each contact position i. The envelope to theses evolutions is also illustrated and named as p_{max}. At step 11,

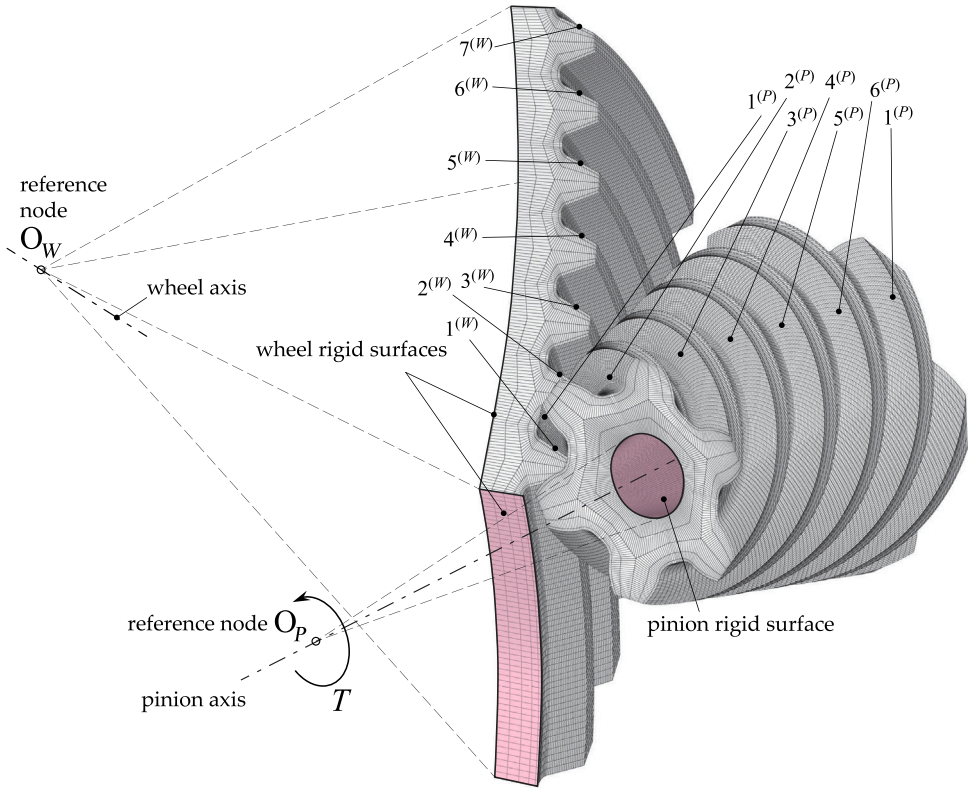

Fig. 10. Finite element model and boundary conditions.

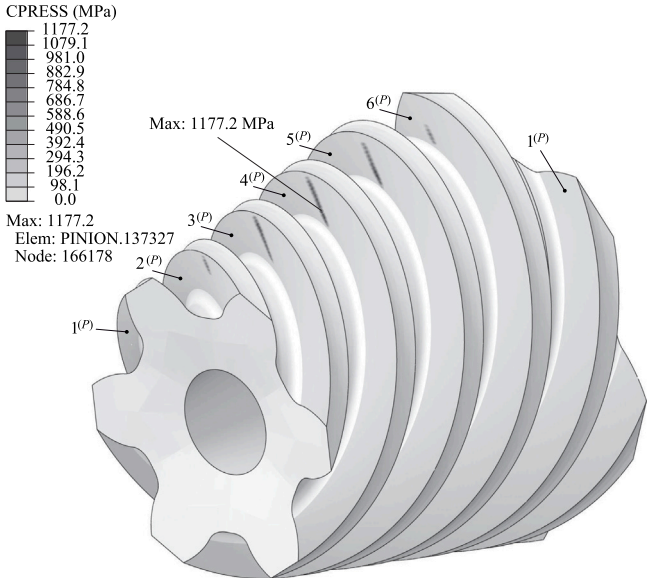

Fig. 11. Formation of the bearing contact on the pinion model and maximum contact pressure at step 11/21 for a torque T = 110 Nm and $a_{tro}^{(P)} = a_{tri}^{(W)} = 0.005\ \text{mm}^{-1}$.

on tooth pair $4^{(P)}$-$4^{(W)}$, the value of 1172.2 MPa, indicated in former Fig. 11, is shown. Fig. 12 shows as well that simultaneous contact occur in four or in five tooth pairs. This circumstance justifies the use of seven teeth in the wheel model to keep the boundary conditions far from the areas of contact.

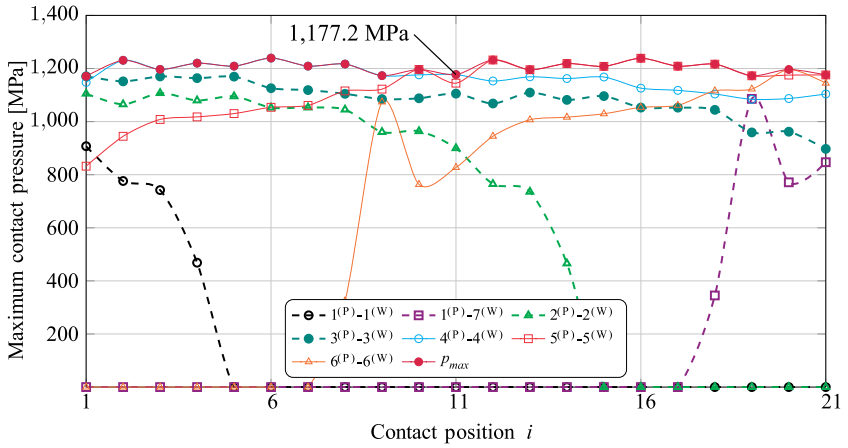

Fig. 12. Evolution of maximum contact pressure at each tooth pair for a torque $T = 110$ Nm and $a_{tro}^{(P)} = a_{tri}^{(W)} = 0.005$ mm^{-1}.

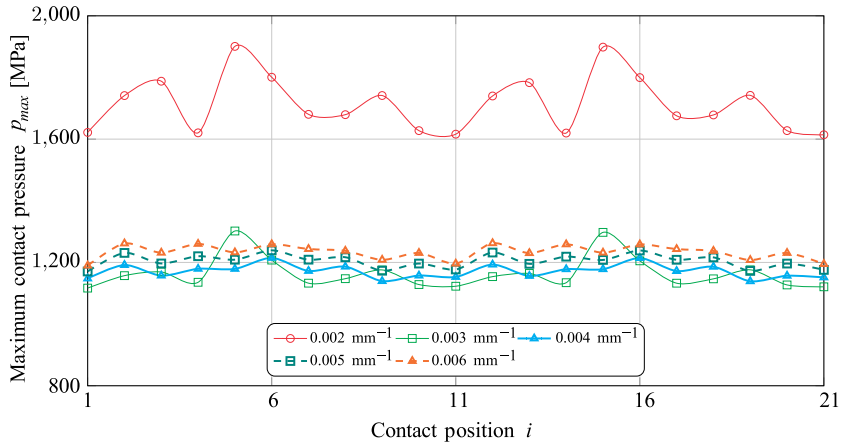

Fig. 13. Comparison of p_{max} for several values of parabola coefficients $a_{tro}^{(P)} = a_{tri}^{(W)}$ when $T = 110$ Nm.

Fig. 13 shows a comparison of the p_{max} for several values of $a_{tro}^{(P)} = a_{tri}^{(W)} = \{0.002, 0.003, 0.004, 0.005, 0.006\}$ mm^{-1}, observing that the optimum value is found for $a_{tro}^{(P)} = a_{tri}^{(W)} = 0.004$ mm^{-1}. A similar optimization could be done for the other rotation of the pinion and considering the nominal torque for this reverse loading situation. In this case, the variables would be the parabola coefficient $a_{tri}^{(P)}$ for the tip relief of the inner blades that generate the pinion convex tooth surfaces, and the parabola coefficient $a_{tro}^{(W)}$ for the tip relief of the outer blades that generates the wheel concave tooth surfaces.

A study of the sensitivity of the gear drive to errors of alignment has been carried out to check the stability of the contact pattern when errors of alignment are presented. This study has been done for the optimum tip relief. Fig. 6 shows the errors of alignment $\Delta\Sigma$, Δa, ΔA_1 and ΔA_2 in a positive direction. Fig. 14 shows the shift of the contact pattern on the radial projection of the pinion concave tooth surface for several values of alignment errors. The considered values are not based in any previous calculation of shaft deflections or gearbox casing deformations. However, they can be considered as high values for a gear drive size with nominal torque of 110 Nm. The gray area allows the visualization of the relative shift of the contact pattern when an error of alignment is presented respect to the expected location of the contact pattern when no errors occur. It can be shown that the contact pattern is quite stable for the different values of alignment errors, showing its larger shift when an axial error of the pinion occurs.

7. Conclusions

The performed research work allows the following conclusions to be drawn:

(1) A methodology to determine the basic machine-tool settings of generated face-hobbed hypoid gears is proposed starting from the definition of the pitch cones. The procedure, based on an exact system of generation, is analytical and direct since it does not require optimization algorithms.

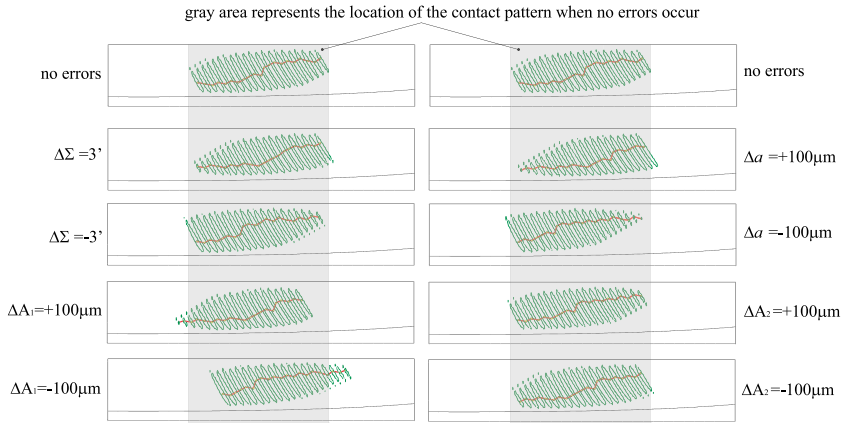

Fig. 14. Relative shift of the contact pattern for several values of errors of alignment.

(2) Application of tooth contact analysis proves that the proposed methodology is actually based on an exact system of generation with conjugate action and no unloaded transmission errors. TCA shows as well that the bearing contact is localized and stable against misalignments.
(3) Stress analysis based on the application of the finite element method shows that the bearing contact requires a small adjustment that can be achieved through the search of the optimum tip relief of the tooth surfaces. The geometries with optimum tip relief show the minimum values of maximum contact pressure along the cycle of meshing.
(4) The methodology has been applied to a high reduction hypoid gear drive with orthogonal axes and considering the Cyclo-Cut as the cutting method. The same problem could be solved considering Cyclo-Palloid as the cutting method. The methodology could be extended to hypoid gear drives with non-orthogonal axes.

Declaration of competing interest

The authors declare that they have no known competing financial interests or personal relationships that could have appeared to influence the work reported in this paper.

Data availability

Data will be made available on request.

Acknowledgments

The authors express their deep gratitude to the Spanish Ministry of Science and Innovation (MCIN) and the Spanish State Research Agency (AEI) for the financial support of research project PID2020-116107GB-I00 (funded by MCIN/AEI/10.13039/501100011033).

Appendix. Basic concepts in a generating face-hobbing process

A computational model for the tooth surfaces of a spiral bevel gear or a hypoid gear that is based on a generating face-hobbing process has been described in several publications [17,29,30]. This section summarizes such a model remarking those variables that have been used in this paper.

A generating face-hobbing process requires basically the definition of the cutter, the positioning of the cutter and the to-be-generated gear in the cutting machine, and the relations of motions between both members.

Fig. A.15 shows a left-hand face-hobbing cutter where outer and inner blades are assembled on the head-cutter with an offset angle π/z_0. Here, z_0 is the number of blade groups. System S_{c1} is used to define the blade profiles of the cutter that generates the pinion. Here, axis x_{c1} points to P_o. Using a similar right-hand cutter (not represented in Fig. A.15), a coordinate system S_{c2} would be defined with its axis x_{c2} pointing to P_i and would allow the definition of the blade profiles of the cutter that generates the wheel.

The slope angle ν defines the orientation of the blades in their assembly on the head-cutter (see Fig. A.15). The slope angle ν is defined as

$$\nu = \arcsin\left(\frac{r_b}{r_{c0}}\right) = \arcsin\left(\frac{m_b z_0}{2r_{c0}}\right) \tag{A.1}$$

where m_b is the blade module and r_{c0} is the cutter radius.

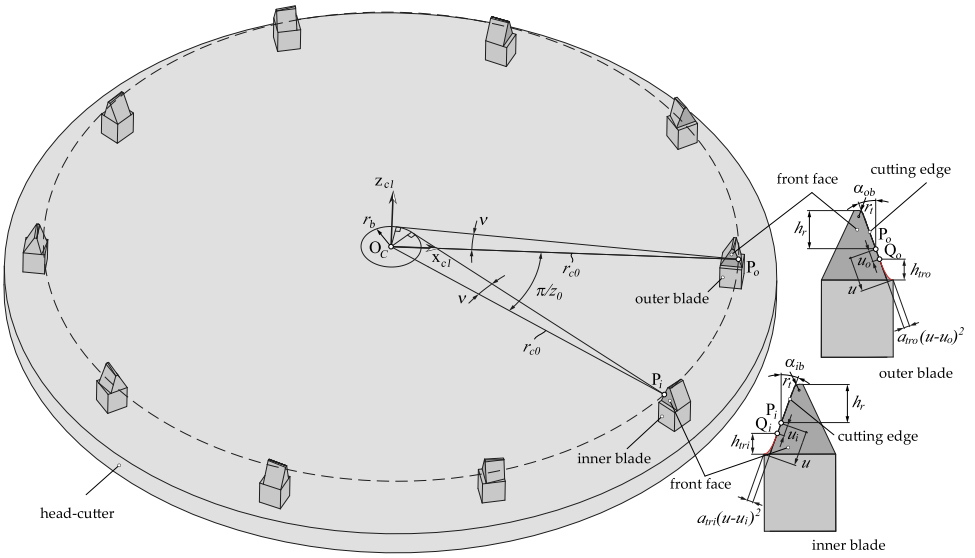

Fig. A.15. Definition of a left-hand face-hobbing cutter.

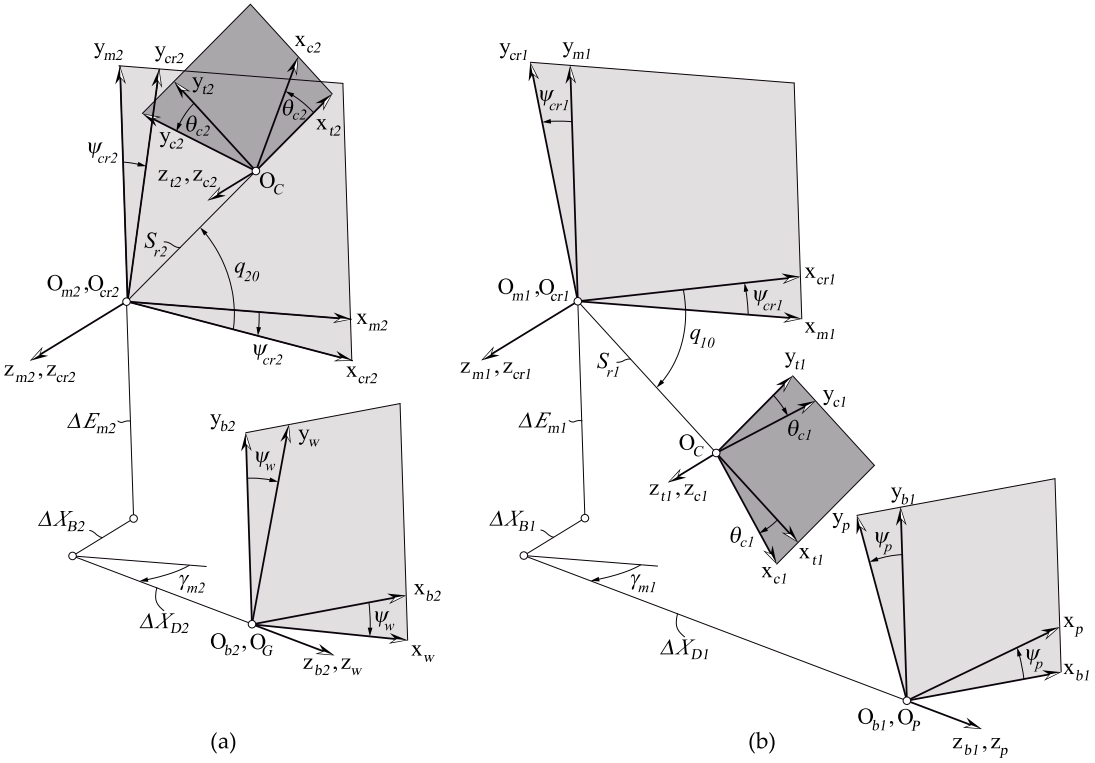

Fig. A.16. Illustration of basic machine-tool settings for: (a) a right hand wheel and (b) a left hand pinion.

The blade pressure angles α_{ib} and α_{ob} are contained in the front planes of the blades since a null rake angle has been considered in this work to simplify the generating process. Otherwise, the blade pressure angle would not be contained in the front plane of the blade and derivation of the profile pressure angle in the front plane would be necessary (see [27]).

The cutting edge is contained in the front plane of the blade and is defined through a profile parameter u (u_1 for the pinion and u_2 for the wheel). A tip relief as the required in this work can be implemented combining a parabola coefficient a_{trb} and a height h_{trb} where $b \equiv i$ for the inner blades and $b \equiv o$ for the outer blades.

The positioning of the head-cutter and the gear (pinion and wheel) in the cutting machine is illustrated in Fig. A.16 for two possible configurations, a right hand wheel and a left hand pinion. Coordinate system S_{ci}, $i = \{1,2\}$, is rigidly connected to the head-cutter that generates the pinion ($i = 1$) or the wheel ($i = 2$). Coordinate systems S_p and S_w are rigidly connected to the to-be-generated pinion and wheel, respectively. Systems S_{m1} and S_{m2} are fixed to the cutting machine.

Pinion and wheel tooth surfaces are obtained by simultaneous observation of the following coordinate transformations

$$\mathbf{r}_p(u_1,\theta_{c1},\psi_{cr1}) = \mathbf{M}_{pb1}(\psi_p(\psi_{cr1},\theta_{c1}))\mathbf{M}_{b1m1}\mathbf{M}_{m1cr1}(\psi_{cr1})\mathbf{M}_{cr1t1}\mathbf{M}_{t1c1}(\theta_{c1})\mathbf{r}_{c1}(u_1) \tag{A.2}$$

$$\mathbf{r}_w(u_2,\theta_{c2},\psi_{cr2}) = \mathbf{M}_{wb2}(\psi_w(\psi_{cr2},\theta_{c2}))\mathbf{M}_{b2m2}\mathbf{M}_{m2cr2}(\psi_{cr2})\mathbf{M}_{cr2t2}\mathbf{M}_{t2c2}(\theta_{c2})\mathbf{r}_{c2}(u_2) \tag{A.3}$$

and the corresponding equations of meshing

$$f_1(u_1,\theta_{c1},\psi_{cr1}) = \left(\frac{\partial \mathbf{r}_p}{\partial u_1}\times\frac{\partial \mathbf{r}_p}{\partial \theta_{c1}}\right)\cdot\frac{\partial \mathbf{r}_p}{\partial \psi_{cr1}} = 0 \tag{A.4}$$

$$f_2(u_2,\theta_{c2},\psi_{cr2}) = \left(\frac{\partial \mathbf{r}_w}{\partial u_2}\times\frac{\partial \mathbf{r}_w}{\partial \theta_{c2}}\right)\cdot\frac{\partial \mathbf{r}_w}{\partial \psi_{cr2}} = 0 \tag{A.5}$$

Here, the following relations are verified

$$\psi_p = \psi_{cr1}m_{1c} + \theta_{c1}\frac{z_0}{z_1} \tag{A.6}$$

$$\psi_w = \psi_{cr2}m_{2c} + \theta_{c2}\frac{z_0}{z_2} \tag{A.7}$$

where m_{1c} and m_{2c} are the velocity ratios for pinion and wheel, respectively.

In (A.2) and (A.3), 4 × 4 order matrices are considered. Their expressions all well known in the specialized literature and are not repeated here. Matrices $\mathbf{M}_{b1m1}$ and $\mathbf{M}_{b2m2}$ depends on the basic machine-tool settings $(\Delta E_{m1}, \Delta X_{B1}, \Delta X_{D1}, \gamma_{m1})$ and $(\Delta E_{m2}, \Delta X_{B2}, \Delta X_{D2}, \gamma_{m2})$, respectively. Additionally, matrices $\mathbf{M}_{cr1t1}$ and $\mathbf{M}_{cr2t2}$ depends on the basic machine-tool settings (S_{r1}, q_{10}) and (S_{r2}, q_{20}), respectively.

References

[1] H.J. Stadtfeld, Introduction to electric vehicle transmissions, Gear Technol. Sep-Oct (2020) 42–50.
[2] R.J. Drago, Gear types and nomenclature, in: Dudley's Gear Handbook, second ed., McGraw-Hill Inc., 1991, pp. 1–49.
[3] A.L. Stewart, E. Wildhaber, Design, Production and Application of the Hypoid Rear-Axle Gear, SAE International, 1926, pp. 386–411, http://dx.doi.org/10.4271/260041.
[4] E. Wildhaber, Basic relationship of hypoid gears, Amer. Mach. (1946).
[5] M.L. Baxter, Basic geometry and tooth contact of hypoid gears, Ind. Math. (1961) 1–28.
[6] ANSI/AGMA ISO 23509-B17, Bevel and Hypoid Gear Geometry, American Gears Manufacturers Association, 2017.
[7] F.L. Litvin, W.S. Chaing, M. Lundy, W.J. Tsung, Design of pitch cones for face-hobbed hypoid gears, J. Mech. Des. 112 (1990) 413–418.
[8] N. Chen, Pitch cone design of face-hobbed hypoid gears, in: Proceedings of the ASME Design Engineering Technical Conferences, Atlanta, 1998, pp. 1–10, http://dx.doi.org/10.1115/DETC98/MECH-5827.
[9] H. Miyamura, Y. Shibata, M. Inagaki, T. Aoyama, Design method for optimizing contact ratio of hypoid gears, in: Proceedings of the ASME Design Engineering Technical Conference, Portland, 2013, pp. 1–7, http://dx.doi.org/10.1115/DETC2013-12761.
[10] G.F. Bär, On optimizing the basic geometry of hypoid gears, Mech. Mach. Theory 104 (2016) 274–286, http://dx.doi.org/10.1016/j.mechmachtheory.2016.06.007.
[11] S. Liu, C. Zhu, A. Fuentes-Aznar, C. Song, Computerized approach for design and generation of face-milled non-generated hypoid gears with low shaft angle, Mech. Mach. Theory 155 (2021) 104084, http://dx.doi.org/10.1016/j.mechmachtheory.2020.104084.
[12] S. Liu, C. Zhu, A. Fuentes-Aznar, C. Song, Computerized determination of the qualified region of main design parameters of face-milled hypoid gears with low shaft angle, Mech. Mach. Theory 159 (2021) 104259, http://dx.doi.org/10.1016/j.mechmachtheory.2021.104259.
[13] C. Liang, C. Song, C. Zhu, F. Cadini, S. Liu, C. Xue, Computational optimization of the basic data and tooth form parameters based on the contact strength for hypoid gear, Mech. Mach. Theory 169 (2022) 104657, http://dx.doi.org/10.1016/j.mechmachtheory.2021.104657.
[14] F.L. Litvin, Y. Zhang, M. Lundy, C. Heine, Determination of settings of a tilted head cutter for generation of hypoid and spiral bevel gears, J. Mech. Transm. Autom. Des. 110 (1988) 495–500, http://dx.doi.org/10.1115/1.3258950.
[15] C.-Y. Lin, C.-B. Tsay, Mathematical model of spiral bevel and hypoid gears manufactured by the modified roll method, Mech. Mach. Theory 32 (1997) 121–136, http://dx.doi.org/10.1016/S0094-114X(96)00043-2.
[16] F.L. Litvin, A. Fuentes, Gear Geometry and Applied Theory, Cambridge University Press, 2004.
[17] Q. Fan, Computerized modeling and simulation of spiral bevel and hypoid gears manufactured by gleason face hobbing process, Trans. ASME, J. Mech. Des. 128 (2006) 1315–1327, http://dx.doi.org/10.1115/1.2337316.
[18] Q. Fan, Tooth surface error correction for face-hobbed hypoid gears, Trans. ASME, J. Mech. Des. 132 (2010) 0110041–0110048, http://dx.doi.org/10.1115/1.4000646.
[19] A. Artoni, A. Bracci, M. Gabiccini, M. Guiggiani, Optimization of the loaded contact pattern in hypoid gears by automatic topography modification, Trans. ASME, J. Mech. Des. 131 (2009) 0110081–0110089, http://dx.doi.org/10.1115/1.3013844.
[20] A. Artoni, M. Gabiccini, M. Kolivand, Ease-off based compensation of tooth surface deviations for spiral bevel and hypoid gears: Only the pinion needs corrections, Mech. Mach. Theory 61 (2013) 84–101, http://dx.doi.org/10.1016/j.mechmachtheory.2012.10.005.
[21] I. Gonzalez-Perez, A. Fuentes, R. Ruiz-Orzaez, An approach for determination of basic machine-tool settings from blank data in face-hobbed and face-milled hypoid gears, Trans. ASME, J. Mech. Des. 137, 093303, http://dx.doi.org/10.1115/1.4031024.
[22] J. Argyris, A. Fuentes, F.L. Litvin, Computerized integrated approach for design and stress analysis of spiral bevel gears, Comput. Methods Appl. Mech. Engrg. 191 (2002) 1057–1095, http://dx.doi.org/10.1016/S0045-7825(01)00316-4.
[23] A. Fuentes-Aznar, R. Ruiz-Orzaez, I. Gonzalez-Perez, Computational approach to design face-milled spiral bevel gear drives with favorable conditions of meshing and contact, Meccanica 53 (2018) 2669–2686, http://dx.doi.org/10.1007/s11012-018-0841-3.
[24] I. Gonzalez-Perez, A. Fuentes-Aznar, Conjugated action and methods for crowning in face-hobbed spiral bevel and hypoid gear drives through the spirac system, Mech. Mach. Theory 139 (2019) 109–130, http://dx.doi.org/10.1016/j.mechmachtheory.2019.04.011.

[25] I. Gonzalez-Perez, A. Fuentes-Aznar, Comparison of cyclo-palloid and cyclo-cut cutting methods for generation of spiral bevel gears, in: Proceedings of the ASME Design Engineering Technical Conference, Cleveland, 2017, pp. 1–10.
[26] H.J. Stadtfeld, Handbook of Bevel and Hypoid Gears: Calculation, Manufacturing and Optimization, Rochester Institute of Technology, 1993.
[27] I. Gonzalez-Perez, A. Fuentes-Aznar, Analytical determination of basic machine-tool settings for generation of spiral bevel gears and compensation of errors of alignment in the cyclo-palloid system, Int. J. Mech. Sci. 120 (2017) 91–104, http://dx.doi.org/10.1016/j.ijmecsci.2016.11.018.
[28] Abaqus Theory Guide, Dassault Systèmes Simulia Corp, United States, 2015.
[29] M. Vimercati, Mathematical model for tooth surfaces representation of face-hobbed hypoid gears and its application to contact analysis and stress calculation, Mech. Mach. Theory 42 (2007) 668–690, http://dx.doi.org/10.1016/j.mechmachtheory.2006.06.007.
[30] Y.P. Shih, Z.H. Fong, G.C. Lin, Mathematical model for a universal face hobbing hypoid gear generator, Trans. ASME, J. Mech. Des. 129 (2007) 38–47, http://dx.doi.org/10.1115/1.2359471.